Vibration control of smart structures using an array of Fiber Bragg Grating sensors

G. Cazzulani *, S. Cinquemani, L. Comolli, A. Gardella, F. Resta

Politecnico di Milano, Dipartimento di Meccanica, Campus Bovisa Sud, via La Masa 1, 20156 Milano, Italy

Received 20 December 2012
Revised 5 June 2013
Accepted 31 July 2013
Available online 19 September 2013

1. Introduction

The widespread use of lightweight structures has emphasized the need to reduce undesired vibrations that can compromise the integrity of the system. Advances in materials technology have made available a new generation of structures regarded as smart. These systems can tune functionality to specific input, for example by changing their shape, stiffness or damping in response to a controllable input [1,2]. To achieve these results, smart structures are instrumented with sensors to evaluate system deformation and actuators to perform control actions [3].

Composite materials are interesting for the construction of smart structures thanks to their high mechanical properties and to the possibility of embedding sensors and actuators. Measurements relating to the structure deformation are used in a control algorithm that is generally based on robust control theory and structural dynamics [4–6]. Depending on the control algorithm, signals are sent to the actuators to generate the desired control forces, whose effect on the structure results in a change of shape, stiffness [7] or damping [8].

One of the most common applications of smart structures is vibration control. This field is interesting especially for lightweight structures, in which vibration phenomena may reduce the fatigue life of structural components [9], and also worsen the functioning of the system, causing discomfort and compromising the safety of people and objects [10].

In this field a sufficiently large number of measurements is preferred to check the state of vibration of the system [11–13]. Moreover, actuators and sensors must be easily integrated in the structure and must offer reduced loading effects [14].

Having a large number of sensors can be technically problematic, but Fiber Bragg Grating sensors (FBG) prove to be an interesting solution for inserting a large number of measuring points on a structure [14–16]. The great advantage of this technology is that a single optical fiber is able to provide a set of measurements of deformation at many points, providing distributed measurement along the structure. The small dimension of the optical fiber and the near absence of load effects make FBG sensors interesting for smart structures [17,18]. In literature, the most common applications of FBGs are structure health monitoring, damage detection and strain measurement in harsh environments[16,19].

One of the first applications of optical fiber sensors for vibration monitoring was presented by Houston in the early nineties [20]. In the following years, several research groups have focused their attention on achieving active control of vibration with FBG sensors. A single sensor was used by Chau and Chuang [21–23] to control the first vibration mode of a cantilever beam. Cheng et al. [24] use an FBG sensor to monitor the vibration of a flexible structure immersed in a fluid. Active vibration control has been implemented on a plate by Ambrosino et al. [25]. Gurses [26] presented an active control using measurements provided by a particular distributed sensor based on optical fiber technology that provides the state of deformation of a strip controlled by PZT actuators. More recently, a resonant inertial actuator with a single embedded FBG sensor was proposed by Cavallo et al. [27].

* Corresponding author. Tel.: +39 02 2399 8430; fax: +39 02 2399 8492.
E-mail address: gabriele.cazzulani@mail.polimi.it (G. Cazzulani).

In this context, the aims of this paper are:

- to extend the results obtained by previous research, exploiting the very high number of measurements made possible by FBG sensors. Thanks to the large number of sensors, a quasi-distributed measurement becomes available and the observation of the vibration phenomenon can be optimized [28–30]. Consequently, the control logics can be improved to achieve their best possible performance. Different control solutions can be introduced depending on the number of sensors and actuators involved in the control algorithm.
- to investigate the possibility of using commercial devices to perform active vibration control, in order to easily extend the results of the research to a large number of practical applications. As a matter of fact, much research in this field is carried out with ad hoc equipment that would be unthinkable in practical applications outside a research laboratory, thus limiting the effectiveness and the interest of the research. On the contrary, a commercial device is already a standard solution and can be profitably used in many practical applications.

The paper is structured as follows. Section 2 recalls the basics of optical fiber and FBG sensor technology, highlighting the advantages of their use in vibration control applications and their limits. Section 3 introduces some control algorithms, based on the increase of structural damping, implemented to demonstrate the effectiveness of FBG sensors in vibration suppression. Section 4 introduces the test bench designed to suppress vibrations using FBG sensors and PZT actuators. The experimental results are presented in Section 5. Tests have been carried out to evaluate the performance of the system with different controllers and different sets of sensors and actuators. Finally conclusions are drawn in Section 6.

2. Optical sensors in vibration control applications

Fiber Bragg Grating sensors, belonging to the optical strain gauges family, are a promising technology in active control applications. The working principle of these sensors is known and it is described in depth in [14], as are the different techniques available to measure the peak shift of the reflected light-wave.

The use of Fiber Bragg Grating sensors in active control of vibrations can be advantageous thanks to the small cross-section that allows them to be embedded in carbon fiber structures with negligible load effects and to the possibility of embedding tens of sensors on the same optical fiber, thus having a large number of measurements without increasing the number and complexity of cables and wiring. Both of these aspects are interesting in vibration control applications, since they provide an insight into the state of deformation of the structure using a non-invasive measurement system. Though the advantages of this technology are evident, there are a number of limitations to its use in applications of vibration suppression that can undermine the effectiveness of control. The main negative factors are related to the delay in the feedback signal due to the processing and the transmission of the signal by the optical interrogator, the discretization of the measurement signal and the resolution of the sensors. In this paper, the effects of these limitations are analyzed and some solutions are presented for exploiting this technology in vibration suppression applications. In the paper, in order to allow the use of technology-based FBG sensors in a large number of potential applications, the intention of the authors is to use only commercial instrumentation. As discussed in the introduction, this allows the results obtained in this work to be extended to a large number of practical applications and sensor configurations. In detail, the signals coming from FBG sensors are acquired using an interrogator based on the *Swept laser* interrogation technique. This interrogator technology, compared with other ones, allows a larger number of sensors (even larger than the number of sensors considered in this paper) to be managed and provides higher flexibility in sensors characteristics (e.g. the wavelength). This means that the number of sensors could be further increased if the structure to be controlled requires an greater number of measurements.

The interrogator adopted is the *MicronOptics SM130-500*. It has a resolution of 1*pm* (corresponding to a strain resolution of 0.84 μm/m) and a sampling frequency of 1 kHz, it has 4 optical channels and manages a maximum number of 80 FBG sensors on each channel. The output is provided through a digital *TCP/IP* Ethernet transmission. The resolution is due to the peak detection and cannot be improved with dynamic interrogators. A better resolution could be obtained only by using static interrogators, but these cannot be used for control applications. As previously mentioned, the main concern with this digital output is the time delay between physical light input and digital data transmission through the Ethernet board. This effect is related to how the peak is measured from the optical spectrum and to the non-deterministic digital Ethernet transmission. To evaluate the acquisition system time delay, tests were done comparing the measurements obtained with both electrical and optical strain gauges applied to the same section of a cantilever beam (Fig. 1a).

The system was excited by a shaker using a sinusoidal input. The mechanical strain is measured simultaneously by the electrical and optical strain gauges. The optical fiber signal is acquired by the interrogator, sent to a PC through the *TCP/IP* connection, acquired through a simple software and outputted to an electrical analog signal by a *DAC* board. The electrical signal is then re-acquired by an acquisition board together with the signal coming from the electrical strain gauges (Fig. 1b). This board, set to 51.2 kHz sampling frequency, is able to guarantee the synchronization of the acquired signals, so that a time delay analysis is possible. To acquire the electrical strain gauges a conditioning module was used. The delay is measured by means of a cross-correlation analysis between the two signals. The results show a delay of (1.7 ± 0.6) ms (Fig. 1c and d). The measured delay includes the interrogator, the *TCP-IP* connection, the software and the *DAC* delay, and represents the total delay due to the use of a digital interrogator. This limitation is difficult to be overcome. Indeed, the use of an interrogator based on different technologies (e.g. linear filter interrogators[25,26]) allows to reduce this delay. Unfortunately this kind of device cannot manage high number of measurements and its use in different applications is limited owing to the high customization of the instrumentation.

A significant contribution, in addition to this delay, is due to the need of low-pass filtering the feedback signal, to avoid high frequency contributions in the control force due to the quantization of the feedback signal. Indeed, the 1 kHz limitation to the feedback loop (due to the sampling frequency of the interrogator) is much lower than the bandwidth of most smart actuators (piezoelectric, magnetostrictive, etc.). For this application, a 4th order 200 Hz Butterworth filter was considered. Since the Butterworth filter phase is almost linear at low frequencies, its behavior can be approximated with a time delay. As a consequence, the average total feedback loop delay in control applications can be calculated as $\delta = 3.6$ ms. Time delay results in a control action phase shift that increases linearly with frequency. As control applications are very sensitive to delays between system vibrations and the corresponding control action (which results in a phase margin reduction), there is a limit to the maximum frequency to be controlled. Considering as acceptable a maximum delay of *0.5* rad, the maximum control frequency can be computed as

$$f_{max} = \frac{1}{2\pi}\frac{0.5}{\delta} \approx 20 \text{ Hz}. \quad (1)$$

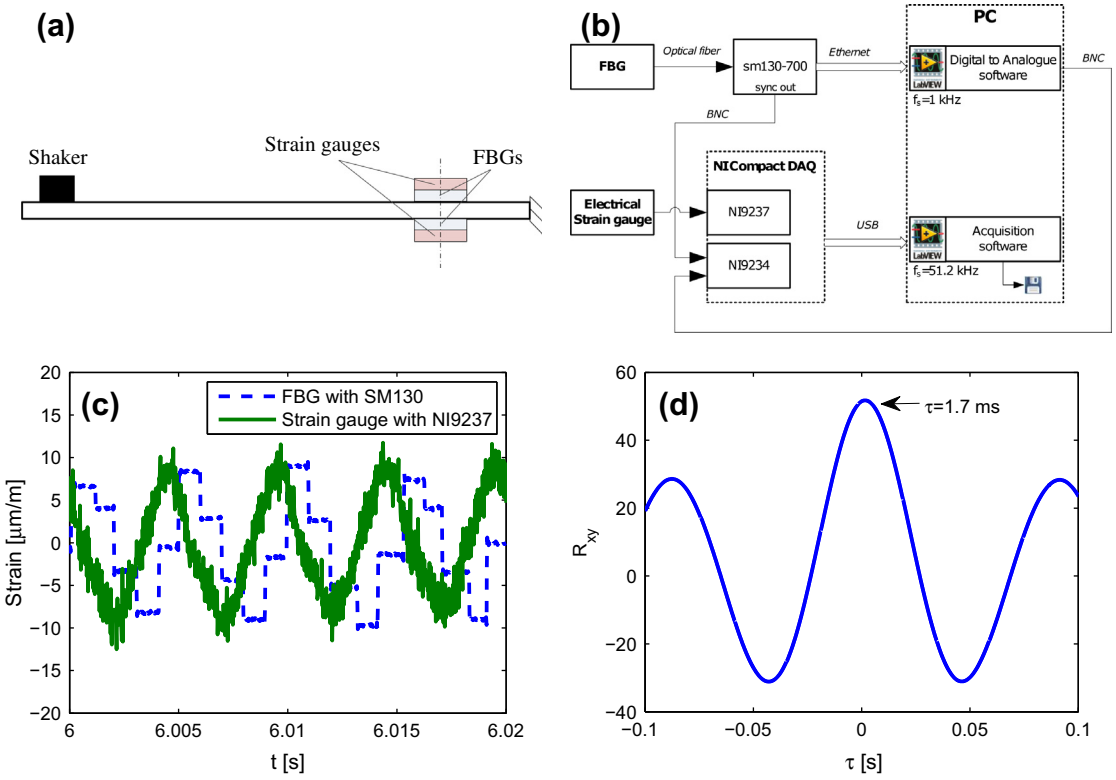

Fig. 1. Analysis of the time delay of optical measurements: (a) the test beam with both optical and electrical strain gauges excited by the shaker; (b) scheme of the acquisition setup; (c) an example of a test signal, a 200 Hz sinusoid; (d) cross-correlation analysis of a band-limited random signal.

This time delay, indeed, depends only on the interrogator architecture, which cannot be modified by the user. In the future and without considering the use of custom equipment (that would preclude the application of this technology in many contexts), this situation could be improved if commercial optical interrogators based on real-time data transmission will be made available.

An alternative solution could be to deal with the time delay in the definition of the control algorithm. Indeed, in literature many researches about this topic can be found. An analysis of the effect of time delay on feedback control can be found in [32,33], while some applications based on the time delay compensation have been proposed [34]. Moreover, some particular control logics based on a delayed feedback of a position [35] or acceleration [36] measurement have been developed. Anyway, all these algorithms present some stability limit and, moreover, they are based on the assumption of known and constant time delay. On the contrary, in this application the delay is caused by non-deterministic data transmission and consequently its value varies in an unknown way over time. For this reason, the use of these logics becomes dangerous from a stability and robustness point of view. Consequently, as described above, the only solution consists in working in a frequency range where the delay introduced in the feedback loop is negligible. Anyway, the introduced frequency limit on the stability of the system is sufficiently high to allow the use of this technology in many mechanical applications in which vibratory phenomena affects low-frequency vibration modes (e.g. [31]).

3. Control techniques

Consider the equation of motion of a linear mechanical system

$$[M]\ddot{\underline{x}} + [R]\dot{\underline{x}} + [K]\underline{x} = [\Lambda_C]^T(\underline{\xi}_C)\underline{F}_C(t) \tag{2}$$

where $[M]$, $[R]$ and $[K]$ are the inertial, damping and stiffness matrices of the structure, $\underline{x}$ is the vector containing the variables describing system motion, while $\underline{F}_C(t)$ is the $n_A \times 1$ vector of control forces (applied at the position $\underline{\xi}_C$) and $[\Lambda_C]$ is the Jacobian matrix linking the forces to the system's degrees of freedom. One of the most efficient ways of reducing vibration is to actively increase system damping and, as a consequence, the energy dissipation associated with it. The control forces can be designed as

$$\underline{F}_c(t) = -[g] \cdot \dot{\underline{\varepsilon}}(\underline{\xi}_S, t) = -[g] \cdot [\Lambda_S(\underline{\xi}_S)] \cdot \dot{\underline{x}}(t) \tag{3}$$

where $\dot{\underline{\varepsilon}}$ is the first derivative of the FBG $n_S \times 1$ measurement vector and $[g]$ is the $n_A \times n_S$ gain matrix, n_A being the number of available actuators and n_S the number of measurements. Vector $\underline{\xi}_S$ represents the position of sensors, while $[\Lambda_S]$ is the Jacobian matrix describing the kinematic relationship between the positions of the n_s sensors and the independent variables $\underline{x}$.

To assess the efficiency of FBG sensors in active vibration control applications, different control algorithms can be considered. The number of actuators (n_A) and sensors (n_S), and their relative position ($\underline{\xi}_S$,$\underline{\xi}_C$), are varied to take into account their effects on control performance.

3.1. Co-located feedback

Supposing that one actuator ($n_A = 1$) and the corresponding co-located sensor ($n_S = 1$) are used, the damping control force F_{c1} is given by

$$F_{c1} = -g_1 \cdot \dot{\varepsilon} \tag{4}$$

where g_1 is the control gain and $\dot{\varepsilon}$ is the first derivative of the FBG measurement. The control gain can be optimized through the root locus of the controlled system to maximize the damping on a certain mode. Theoretically, under the assumption of no noise, no delays, ideal actuators, etc., this solution ensures the stability of the controlled system for any value of the control gain, even if, in prac-

tice it is very common to have problems of signal noise, or related to the A/D conversion, delays, etc.

In order to increase the signal-to-noise ratio and improve the performance of control on the selected modes, supposing one actuator ($n_A = 1$) is used, an increased number of sensors can been considered. For example, considering the co-located sensor (ith FBG) and the two adjacent ones ($n_S = 3$), the control action becomes

$$F_{c1} = -[g_1 \quad g_2 \quad g_3] \cdot \begin{bmatrix} \dot{\varepsilon}_{i-1} \\ \dot{\varepsilon}_i \\ \dot{\varepsilon}_{i+1} \end{bmatrix} \tag{5}$$

where g_1, g_2, g_3 are the control gains associated to each measurement. By tuning the control gains, it is possible to vary the damping effect achieved on the different modes with respect to (4), obtaining a better result on the most critical modes.

Both (4) and (5) can be extended to a higher number of control actuators. For example, considering two control actuators ($n_A = 2$), (4) can be expressed as

$$\begin{bmatrix} F_{c1} \\ F_{c2} \end{bmatrix} = -\begin{bmatrix} g_1 & 0 \\ 0 & g_2 \end{bmatrix} \cdot \begin{bmatrix} \dot{\varepsilon}_i \\ \dot{\varepsilon}_j \end{bmatrix} \tag{6}$$

where ε_i, ε_j are the measurements of the sensors co-located with the actuators providing the control forces F_{c1} and F_{c2}, while g_1, g_2 are their control gains. Similarly, (5) becomes

$$\begin{bmatrix} F_{c1} \\ F_{c2} \end{bmatrix} = -\begin{bmatrix} g_{11} & g_{12} & g_{13} & 0 & 0 & 0 \\ 0 & 0 & 0 & g_{21} & g_{22} & g_{23} \end{bmatrix} \cdot \begin{bmatrix} \dot{\varepsilon}_{i-1} \\ \dot{\varepsilon}_i \\ \dot{\varepsilon}_{i+1} \\ \dot{\varepsilon}_{j-1} \\ \dot{\varepsilon}_j \\ \dot{\varepsilon}_{j+1} \end{bmatrix} \tag{7}$$

where F_{c1} and F_{c2} are the two control forces and i, j the indices of the sensors co-located with the actuators. Results being equal, the use of multiple actuators allows the forces acting on the structure to be reduced and avoids saturation of the actuators. Moreover, having an higher number of independent control parameters, it is possible to tune them in order to maximize the damping on more than one controlled mode.

3.2. Modal feedback

To better exploit all the n_S measurements available using optical strain gauges, Modal Control [6,31] can be implemented. An in depth description of modal control techniques is described in [6]. To calculate the control forces, the modal-space equation of motion can be defined starting from (2) through the coordinate change

$$\underline{x} = [\Phi_{tot}]\underline{q}_{tot} \tag{8}$$

where $\underline{q}_{tot}$ is the vector containing all the structure modes and $[\Phi_{tot}]$ is the eigenvector matrix of $[M]^{-1}[K]$. In most practical cases, (8) can be truncated considering only a limited number of modes (m) for the definition of the control law, since only a limited frequency range is affected by significant vibration phenomena. In this case, (8) becomes

$$\underline{x} \simeq [\Phi]\underline{q} \tag{9}$$

where $\underline{q}$ is the $m \times 1$ vector containing only the modes considered, while $[\Phi]$ is the $n_{dof} \times m$ corresponding eigenvector matrix. Substituting (9), (2) becomes

$$[diag_M]\ddot{\underline{q}} + [diag_R]\dot{\underline{q}} + [diag_K]\underline{q} = [\Phi]^T[\Lambda_C]^T\underline{F}_C(t) \tag{10}$$

where $[diag_M]$,$[diag_R]$ and $[diag_K]$ are the modal diagonal inertia, damping and stiffness matrices (defined as $[\Phi]^T[M][\Phi]$, etc.). This equation represents a series of decoupled equations, each one representing the dynamics associated with one structure mode. When Independent Modal Space Control (IMSC) is applied, control forces can be calculated as

$$\underline{F}_C = -\left([\Phi]^T[\Lambda_C]^T\right)^{-1}[\bar{r}]\dot{\underline{q}} = -\left([\Phi]^T[\Lambda_C]^T\right)^{-1}[\bar{r}]([\Lambda_M][\Phi])^+\dot{\underline{\varepsilon}} \tag{11}$$

where $[\bar{r}]$ is the $m \times m$ modal control gain matrix (whose elements correspond to the damping introduced by the control on the m controlled modes) and $[\,\cdot\,]^+$ is the $m \times n_S$ pseudo-inverse matrix. The pseudo-inverse matrix allows measurement noise to be filtered out since it provides the least squares solution of a system of linear equations minimizing the Euclidean norm $\left\|[\Lambda_M][\Phi]\dot{\underline{q}} - \dot{\underline{\varepsilon}}\right\|_2$. Having more measurements, errors in estimation of modal quantities $\dot{\underline{q}}$ can be minimized.

4. Experimental setup

To assess the proposed control layout, a test bench structure with embedded FBG sensors was created. The structure (Fig. 2) is a carbon fiber clamped-free beam, instrumented with an array of 16 embedded FBG sensors and 3 piezoelectric actuators.

Its dimensions are 850 mm × 105 mm × 1.7 mm and it is constructed from three layers of *prepreg* unidirectional carbon fiber. The *prepreg* is a composite material made of carbon fiber immersed in a partially polymerized epoxy matrix. To achieve full lamination of the layers and reach high mechanical properties, the material must be subjected to a process of *curing*, after which the carbon fiber reaches a nominal density of 2000 kg/m^3 and a Young modulus of 110 GPa along the direction of the fibers. Piezoelectric actuators used to control vibrations are QP20W produced by *Midé*. A chain of FBG sensors on the same optical fiber is selected, with 16 equally spaced gratings, both in distance (60 mm) and wavelength (4.7 nm, from 1515 nm to 1585 nm). Each sensor has a grating length of 8 mm, with a peak reflectivity of 20%. Only the first 14 gratings are used for control purposes, while the other 2 are used for temperature compensation. Table 2 summarizes the main features of the FBG sensors used, while Table 1 shows the characteristics of the piezoelectric actuators.

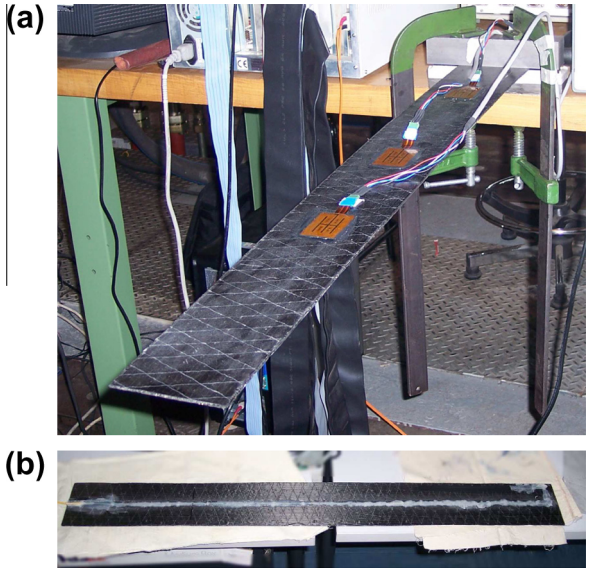

Fig. 2. A picture of the smart structure (a) and its bottom-side with optical fiber FBG sensors (b).

Table 1
Technical data of the QP20w piezoelectric actuator.

Dimensions	$0.0508 \times 0.0381 \times 7.62 \cdot 10^{-4}$	m^3
Mass	0.0079	kg
Electrode dimensions	$0.0460 \times 0.0333 \times 2.54 \cdot 10^{-4}$	m^3
Capacity	$0.20 \cdot 10^{-6}$	F
Voltage	±200	V
Young modulus	63,000	MPa
Maximum operating temperature	100	°C

Table 2
Main features of the adopted FBG sensors (source Fos&S).

Operating temperature	−50 to +130	°C
Grating length	0.008	m
Coating diameter	$195 \cdot 10^{-6}$	m
Coating material	Ormocer	
Strain range (long term)	0.01	m/m
Strain range (short term)	0.05	m/m
Accuracy (with a 1 pm accuracy interrogator)	$1.7 \cdot 10^{-6}$	m/m

4.1. Placement of sensors and actuators

The placement of sensors and actuators was effected bearing in mind that they respectively sense and produce a deformation of the curvature of the system. In fact, the action of a piezoelectric patch actuator can be modeled as two opposite torques acting on the two endpoints of the patch. The actuator, then, works on the difference of rotation between these points, which is related to curvature. Similarly, FBG sensors measure a linear deformation of the structure which is a function of the curvature and of the distance from the neutral axis. Their optimal positioning then corresponds to the points where the second derivative of the vibrational modes is maximum. Fig. 3 shows the first three analytical modal shapes $\phi_i(\xi)$ of the structure. The position of the actuators is chosen so that each PZT is co-located with one of the FBG sensors. Moreover, at least one PZT is placed, for each mode, in a position with non-zero curvature to ensure the controllability of the system.

The efficiency of both actuators and sensors is guaranteed as long as they adhere perfectly to the structure. The experience gained in previous work suggested the use of structural adhesive *3M DP490* to bond piezoelectric actuators, while optical fiber are bonded using the two-component glue *HBM X60* [37].

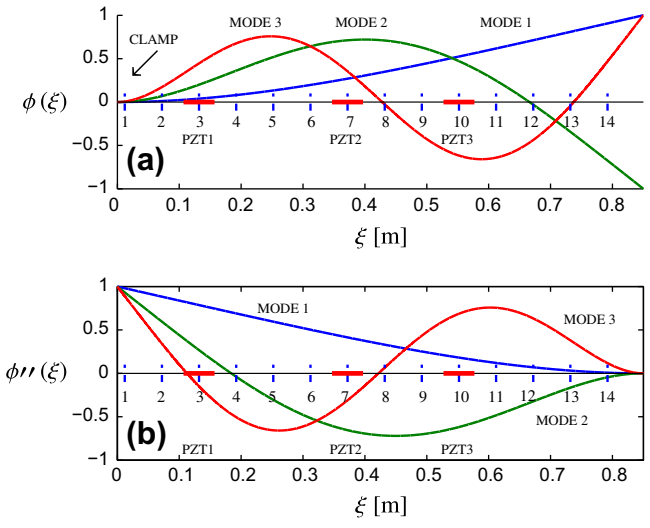

Fig. 3. Position of actuators (PZT) and sensors with respect to the normalized numerical modal shapes (a) and curvature (b) of the structure constrained as a cantilever beam.

4.2. System identification and numerical model

The large number of available measurement points is a great potential which, to be fully exploited, needs a numerical model describing the dynamics of the system. Such a model provides a relationship between the measurements obtained by sensors and the effect of actions applied by the actuators. The system is discretized with a Finite Element Method (FEM) mesh of 36 nodes. Each node can translate and rotate in the plane. The first node is fixed to the ground, then the model has a total of 105 degrees of freedom.

FBG sensors are modeled approximating the deformation sensed with the difference of rotation $\Delta\theta$ of two adjacent nodes, placed at the ends of the sensor itself. Similarly, PZT actuators are modeled as two torques applied on the nodes placed at the ends of the devices. Fig. 4a shows the mesh of the system, highlighting a sector of the beam with both actuator and sensor. Fig. 4b–d shows the comparison between analytical, numerical and experimental modal curvatures of the first three modal shapes along the beam. The vertical axes represent the curvature of each modal shape, normalized so that the modal curvature on the second FBG sensor is equal to 1. The horizontal axes, whose ticks are the sensors' number (from 1 to 14) represents the beam length. Sensor 1 is the sensor closest to the clamp, while sensor 14 is close to the beam tip.

The system has been modeled in two different ways. The analytical model has uniform characteristics along the structure and then does not include the local stiffening effect due to the actuators [1]. On the contrary the finite element model is more detailed and includes this effect. A good match between numerical and experimental modes can be observed. As the local stiffening effect introduced by the PZT patches (not included in the analytical model) have not been modeled, the analytical model shows differences with respect to experimental results especially in points where the PZT actuators are placed (FBG3, FBG7 and FBG10).

At the same time, to determine experimentally the natural frequencies of the structure, actuator PZT3 was used to force the system, while sensor FBG1 senses the state of deformation. The experimental transfer function $G_{13}(s) = \frac{\varepsilon_1(s)}{V_3(s)}$ between the voltage V_3 applied to the actuator PZT3 and the deformation ε_1 measured by the sensor FBG1 is shown in Fig. 5. The first three vibrational modes of the structure are clearly visible both in magnitude and in phase diagrams.

Fig. 5 shows the comparison between experimental and numerical transfer functions $G_{13} = \frac{\varepsilon_1}{V_3}$, computed through the H1 estimator, and the eigenfrequencies and non-dimensional damping of the numerical model. The phase shift between the numerical and experimental data (increasing with the frequency) is due to the time delay of the FBG measurement (not included in the numerical model). Anyway, except for this, the differences are very small and the model can be considered valid to describe the dynamics of the system.

5. Results and discussion

The control logics described in Section 3 were tested on the smart structure. Fig. 6 shows the scheme of the control loop, highlighting the elements involved in the control. Vibrations are measured by FBG sensors and acquired through the optical interrogator. The signals are transmitted through the ethernet connection to a PC, used as control board. A custom software acquires these measurements, calculates the control signals and provides

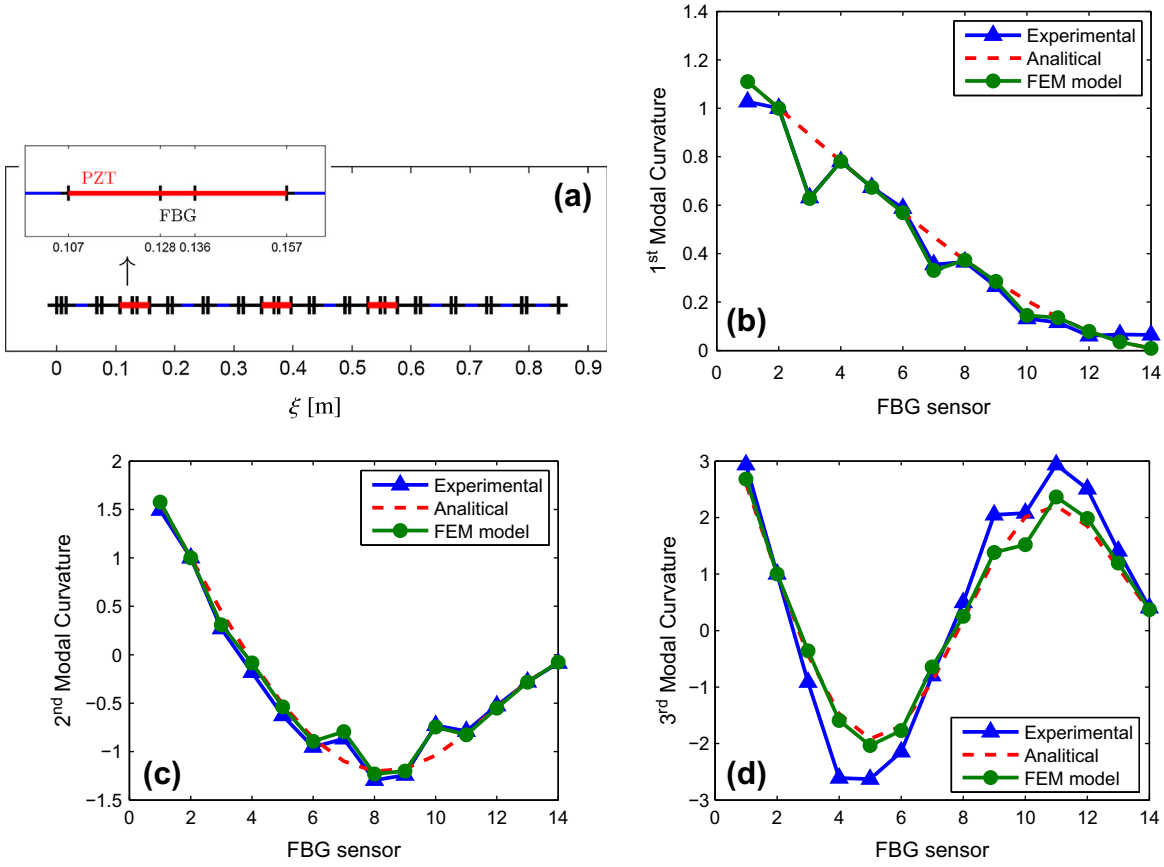

Fig. 4. Finite element model of the system: nodes (a) and numerical-experimental comparison of mode 1 (b), 2 (c) and 3 (d).

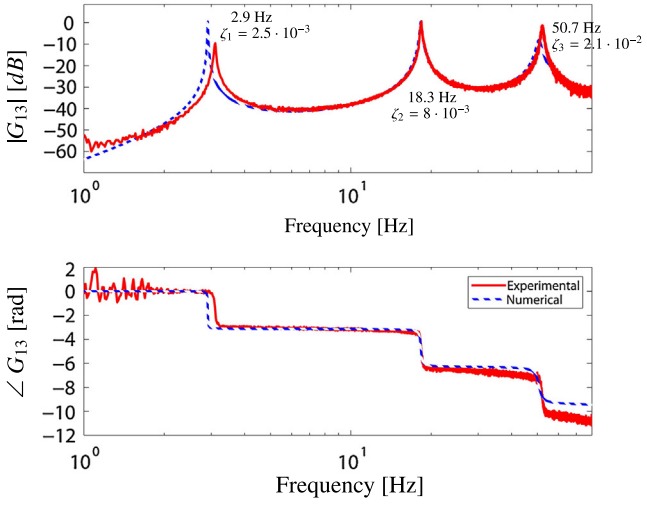

Fig. 5. Numerical and experimental transfer functions between PZT3 and FBG1; the shown values refer to the numerical model.

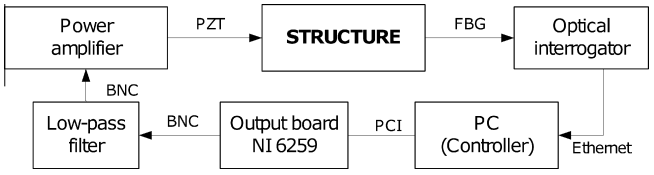

Fig. 6. Block diagram of the control loop.

them as output through a National Instruments NI6259 board. The control signals are low-pass filtered, to cancel out the high frequency contributions due to the signal quantization, amplified and provided to the piezoelectric patch actuators.

The control strategies previously discussed are tested to evaluate the performance of a smart structure with embedded FBG sensors in active vibration control application. For all the tests, the third piezoelectric actuator (PZT3) is used to provide a disturbance input (a chirp signal from 1 to 60 Hz in 600 s, covering the frequency range of the controlled modes and of the first uncontrolled one), while the third sensor (FBG3) is used to evaluate control performance. Owing to the frequency limitation caused by the delay of the control chain, only the first and the second modes of the system are controlled.

The co-located control, described by (4), was realized considering the third sensor (FBG3) and the first actuator (PZT1). Fig. 7a and b represents the root locus with co-located control, showing the poles of the first two modes of the controlled structure varying the control gain. The poles corresponding to the control gain maximizing the damping on the first mode (3.5%) are represented by a red star, while those maximizing second mode damping (2.1%) are represented by a green star. As shown by the figure, each of these gains does not provide a good result on the other mode; for this reason, the control gain has been chosen so that both the 1st and 2nd modes are provided with the same damping (1.85%, corresponding to the "+" in the figure). As said in the preceding paragraphs, the performance of this simple logic is limited also by the resolution and signal-to-noise ratio of the FBG sensors. However more than one sensor can be used to define the control force (see (5)). Sensors FBG2 to FBG4 are considered, while the feedback action is still provided by the PZT1 actuator. Fig. 7c and d shows

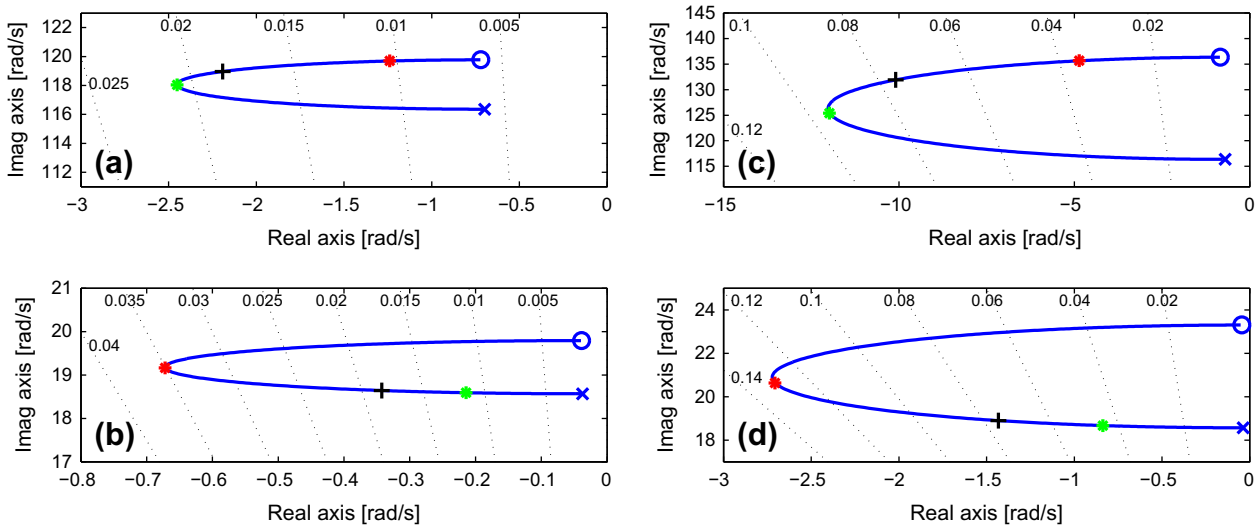

Fig. 7. Root locus of the structure with SISO co-located control (2nd mode (a) and 1st mode (b)) and for the 1-actuator, 3-sensors case (2nd mode (c) and 1st mode (d))

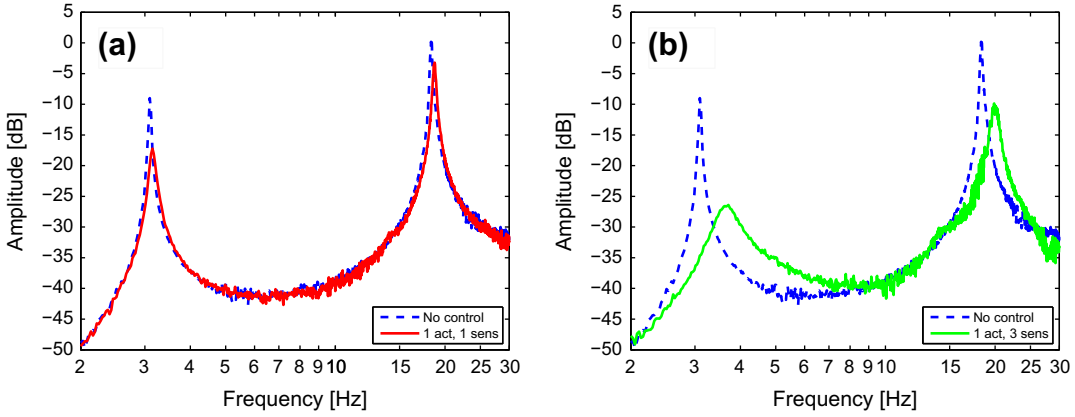

Fig. 8. Comparison between controlled and uncontrolled system in terms of FRF magnitude with co-located control (a) and with 3-sensor co-located control (b).

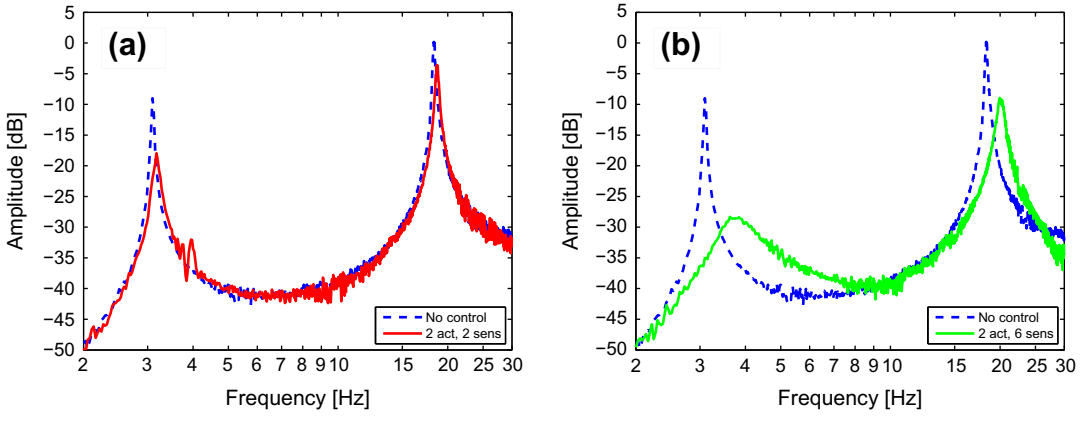

Fig. 9. Comparison between controlled and uncontrolled system in terms of FRF magnitude with 2 sensors – 2 actuators co-located control (a) and with 6 sensors – 2 actuators control (b).

the root locus of the first two modes for this solution. The root locus has been designed for a given relative weight of the 3 sensors, following the same notation of Fig. 7a and b: the black "+" represent the poles corresponding to the chosen gains.

Fig. 8a shows the comparison between the controlled and the uncontrolled system for the co-located control in terms of frequency response function between the input voltage of the disturbance piezoelectric patch and the measurement of the third FBG

sensor. The result shows a peak reduction corresponding, on the first mode, to a damping ratio increase from 0.2% to 1.8%. This value is consistent with the result shown by the root locus diagram. On the contrary, owing to the higher phase delay, the result on the second mode is less effective than expected. Fig. 8b shows the performance of this solution. A damping ratio of 7% can be achieved on the first mode, leading to an high improvement of vibration reduction with respect to the previous case. A higher frequency shift, due to the higher control force, can also be observed.

Control performance can be improved using more actuators. This solution allows the control force provided by the single actuator to be reduced, thus limiting the risk of saturation and a concentrated force on a single point of the structure. The following results are obtained controlling the system with the two actuators PZT 1 and 2 and the corresponding co-located sensors (see (6) and (7)). Fig. 9 shows the result of this control solutions. Comparing it with Fig. 8, it can be noticed that the actuator PZT2 does not provide a significant contribution to vibration reduction.

As expected, the results achieved show that an increase of the number of sensors allows vibration control performance to be improved. In this sense, FBG sensors offer a great advantage compared with other sensors (accelerometers, piezoelectric sensors, etc.) since they can be embedded in the structure in large number. However, increasing the number of considered sensors and the complexity of the structure, a simple velocity feedback can be difficult to use, since the contribution of each mode is unknown and, as a consequence, it is difficult to define the weights for the feedback forces.

When the system is complex and vibration phenomena interest more modes, it has been shown that IMSC is an effective algorithm for reducing vibrations exploiting the high number of sensors

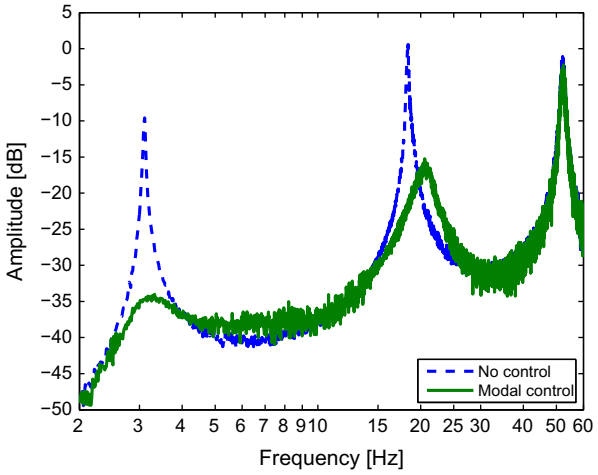

Fig. 10. Effect of IMSC application on the first and second modes of the beam in terms of FRF magnitude. The third mode was not controlled.

Table 3
Comparison of control performances in terms of peak reduction [dB] on first and second mode.

Control algorithm	Peak reduction [dB]	
	Mode 1	Mode 2
co-located feedback, 1 actuator, 1 sensor	7.4	3
co-located feedback, 1 actuator, 3 sensors	16.6	9.3
co-located feedback, 2 actuators, 2 sensors	8	3.4
co-located feedback, 2 actuators, 6 sensors	15	9.3
modal feedback, 2 actuator, 14 sensors	24	16

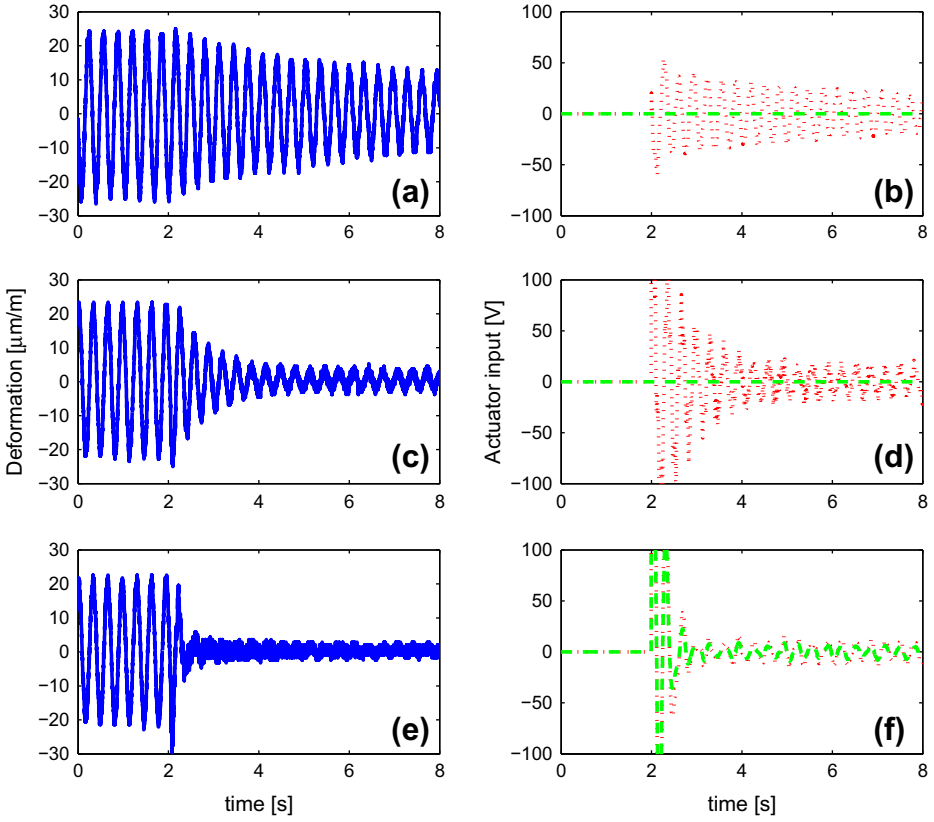

Fig. 11. Comparison between controlled and uncontrolled structure in time domain on the first mode: 1 sensor-1 actuator case (a,b), 3 sensors-1 actuator case (c,d) and modal control (e,f). The solid blue line (on the left) refers to the FBG1 time history, while the dotted red line and the dashed green one (on the right) refer to the PZT1 and PZT2 control inputs respectively. (For interpretation of the references to colour in this figure legend, the reader is referred to the web version of this article.)

available. In this application (see Section 4) 14 FBG sensors, equally distributed along the beam, are available and all of them were used to estimate the system modal coordinates. Owing to the frequency limitations of this control scheme (see Section 2) the first two modes of the beam were controlled.

Fig. 10 shows the frequency response function between the disturbance piezoelectric patch input voltage and the 3 s FBG sensor when IMSC is applied. A target damping ratio of 20% has been imposed for the controlled modes and, as a consequence, considerable reduction of system vibrations can be achieved. In the experimental tests, the first mode damping ratio becomes 19% (a value comparable with the imposed one) while the second mode one becomes 6%. Thanks to the large number of sensors, the spillover problem does not arise and third mode behavior is not worsened by control. As expected, control performance on the first mode is better, both in terms of damping increase and frequency shift, owing to the lower delay of the control feedback at lower frequencies.

Table 3 summarizes the performance of the control logics tested in terms of peak reduction achieved on the first and second mode, while Fig. 11 shows a comparison between the different controls in the time domain. The results were obtained exciting the structure at its first natural frequency with the PZT3 actuator. In all the tests, the system remains uncontrolled in the first two seconds and then the control is switched on. The figure compares the results obtained in terms of time histories of FBG1 (on the left) and actuators control input voltage (on the right). Both Table 3 Fig. 11 confirm that the increase of the number of sensors and actuators, fully exploited with IMSC, allows a significant reduction of vibrations on both the controlled modes. As expected, the peak reduction on first mode is always higher than the reduction on the second, owing to the lower phase delay of the control force at lower frequencies.

6. Conclusions

The possibility of building lightweight structures that can actively change their mechanical properties (e.g. damping) is of great interest. This work demonstrates the possibility of creating a smart structure, made of carbon fiber, with embedded arrays of FBG sensors for active vibration control. The system is able to reduce low frequency vibration by increasing system structural damping.

This was investigated as a function of the implemented control logic and of the number of sensors and actuators used.

Experimental tests were carried out to evaluate control performances considering different numbers of actuators and FBG sensors. The most significant results are achieved by implementing Independent Modal Space Control. In fact, thanks to the large number of FBG sensors available, this technique is very effective since it allows a distributed measurement of system deformation, providing an estimate of modal coordinates and avoiding the occurrence of unwanted spillover effects.

References

[1] Vepa R. Dynamics of smart structures. John Wiley Sons Ltd; 2010.
[2] Wagg D, Bond I, Weaver P, Friswell M. Adaptive structures engineering applications. John Wiley Sons Ltd; 2007.
[3] Chopra I. Review of state of art of smart structures and integrated systems. AIAA J 2002;40(11):2145–87.
[4] Meirovitch L, Baruh H, Oz H. A comparison of control techniques for large flexible systems. J Guid Control 1983;6(4):302–10.
[5] Balas MJ. Active control of flexible systems. J Optim, Theory Appl 1978;25(3):415–36.
[6] Braghin F, Cinquemani S, Resta F. A new approach to the synthesis of modal control laws in active structural vibration control. J Vib Control 2013;19(2):163–82.
[7] Ghoshal A, Wheater EA, Kumar CRA, Sundaresan MJ. Vibration suppression using a laser vibrometer and piezoceramic patches. J Sound Vib 2000;235:26180.
[8] Balas M. Direct velocity feedback control of large flexible structures. J Guid Control 1979;3(2):252–3.
[9] Hyer MW. Stress analysis of fiber-reinforced composite materials. New York: WCB/McGraw-Hill Inc; 1998.
[10] Cazzulani G, Ghielmetti C, Giberti H, Resta F, Ripamonti F. A test rig and numerical model for investigating truck mounted concrete pumps. Automat Construct 2011;20(8):1133–42.
[11] Khulief YA. Vibration suppression in rotating beams using active modal control. J Sound Vib 1985;242(4):681–99.
[12] Inman DJ. A comparison of control techniques for large flexible systems. Philos Trans: Math Phys Eng Sci 2002;359(1778):205–19.
[13] C Hughes P, E Skelton R. Controllability and observability of linear matrix second order systems. ASME J Appl Mech 1980;47:415–20.
[14] V Grattan KT, Sun T. Fiber optic sensor technology: an overview. Sens Actuat A: Phys 2000;82(1–3):40–61.
[15] Othonos A. Fiber bragg gratings. Rev Sci Instrum 1997;68(12):4309.
[16] Kreuzer M. Strain measurement with Fiber Bragg Grating sensors. HBM; 2006.
[17] Luyckx G, Voet E, De Waele W, Degrieck J. Multi-axial strain transfer from laminated CFRP composites to embedded Bragg sensor: I. Parametric study. Smart Mater Struct 2010;19.
[18] Udd E. Fiber optic smart structure. Proc IEEE 1996;84(1).
[19] Comolli L, Bucca G, Bocciolone M, Collina A. First results from in line strain measurements with FBG sensors on the pantograph collector of underground trains. In: Proceedings of photonics Europe Bruxelles, Belgium; 2010.
[20] Huston DR, Fuhr PL, Beliveau JG, Spillman WB. Structural member vibration measurements using a fiber optic sensor. J Sound Vib 1991;149:348–53.
[21] Chau K, Moslehi B, Song G, Seth V. Experimental demonstration of Fiber Bragg Grating strain sensors for structural vibration control. In: Proceedings of SPIE 753-64; 2004.
[22] Chuang KC, Ma CC, Liao HT. A point-wise fiber Bragg grating displacement sensing system and its application for active vibration suppression of a smart cantilever beam subjected to multiple impact loadings. Smart Mater Struct 2012;21(6). art. no. 065003.
[23] Chuang KC, Ma CC, Wu RH. Active suppression of a beam under a moving mass using a pointwise fiber bragg grating displacement sensing system. IEEE Trans Ultrason Ferroelectr Freq Control 2012;59(10):2137–48.
[24] Cheng L, Zhou Y, Zhang MM. Controlled vortex-induced vibration on a fix-supported flexible cylinder in cross-flow. J Sound Vib 2006;292(1–2):279–99.
[25] Ambrosino C, Diodati G, Laudati A, Gianvito A, Concilio A, Sorrentino A, et al. Active vibration control using fiber Bragg grating sensors and piezoelectric actuators in co-located configuration. In: Proceedings of SPIE, art no. 661940; 2008.
[26] Gurses K, Buckham BJ, Park EJ. Vibration control of a single-link flexible manipulator using an array of fiber optic curvature sensors and PZT actuators. Mechatronics 2009;19(2):167–77.
[27] Cavallo A, May C, Minardo A, Natale C, Pagliarulo P, Pirozzi S. Active vibration control by a smart auxiliary mass damper equipped with a fiber Bragg grating sensor. Sens Actuat A: Phys 2009;153(2):180–6.
[28] Rapp S, Kang LH, Han JH, Mueller UC, Baier H. Displacement field estimation for a two-dimensional structure using fiber Bragg grating sensors. Smart Mater Struct 2009;18(2). art. no. 025006.
[29] Kim HI, Kang LH, Han JH. Shape estimation with distributed fiber Bragg grating sensors for rotating structures. Smart Mater Struct 2001;20(3). art. no. 035011.
[30] Jiang H, Van Der Veek B, Kirk D, Gutierrez H. Real-time estimation of time-varying bending modes using fiber bragg grating sensor arrays. AIAA J 2013;51(1):178–85.
[31] Resta F, Ripamonti F, Cazzulani G, Ferrari G. Independent modal control for nonlinear flexible structures: an experimental test rig. J Sound Vib 2010;329(8):961–72.
[32] Ramachandran P, Ram YM. Stability boundaries of mechanical controlled system with time delay. Mech Syst Signal Process 2012;27(1):523–33.
[33] Peng J, Wang L, Zhao Y, Zhao Y. Bifurcation analysis in active control system with time delay feedback. Appl Math Comput 2013;219(19):10073–81.
[34] Shao MQ, Chen WD. Active vibration control in a cantilever-like structure: a time delay compensation approach. JVC/J Vib Control 2013;19(5):674–85.
[35] Hosek M, Olgac N, Elmali H. The centrifugal delayed resonator as a tunable torsional vibration absorber for multi-degree-of-freedom systems. JVC/J Vib Control 1999;5(2):299–322.
[36] Qiu ZC, Han JD, Zhang XM, Wang YC, Wu ZW. Active vibration control of a flexible beam using a non-collocated acceleration sensor and piezoelectric patch actuator. J Sound Vib 2009;326(3–5):438–55.
[37] Comolli L, Micieli A. Numerical comparison of peak detection algorithms for the response of FBG in non-homogeneous strain fields. In: Proceedings of optical fiber sensors (OFS-21), Ottawa, Canada; 2011.